ISSN 1063-7788, Physics of Atomic Nuclei, 2024, Vol. 87, Suppl. 3, pp. S409–S417. © Pleiades Publishing, Ltd., 2024.

NUCLEI
Experiment

Experimental Study of Interaction of the Proton and Deuteron with the Atomic Nuclei of Lithium and Boron

G. M. Ostreinov[1]*, S. Yu. Taskaev[1], Ia. M. Kolesnikov[1], E. O. Sokolova[1], T. A. Bykov[1], D. A. Kasatov[1], M. I. Bikchurina[1], and S. S. Savinov[1]

[1] *Budker Institute of Nuclear Physics, Siberian Branch, Russian Academy of Sciences (BINP SB RAS), 630090, Novosibirsk, Russia*

Received November 27, 2024; revised December 17, 2024; accepted December 17, 2024

Abstract—At the electrostatic accelerator at the Institute of Nuclear Physics, the differential cross-sections of nuclear reactions with deuteron and proton beams on light nuclei in the energy range of 0.3–2.2 MeV were measured by α-detector.

DOI: 10.1134/S1063778824701059

1. INTRODUCTION

In this paper, we measured the differential cross sections of the following three groups of reactions: $d + \mathrm{Li}$, $p + {}^{11}\mathrm{B}$ and $d + {}^{10}\mathrm{B}$.

In the first group of reactions, there are ten channels when a deuteron interacts with a lithium nucleus, five of which lead to the generation of neutrons. The highest neutron yield is provided by the $\mathrm{Li}(d,n)$ reaction starting with the energy of 1 MeV. This interaction results in the production of neutrons, protons, tritium, ${}^3\mathrm{He}$, α-particles, ${}^7\mathrm{Li}$, and ${}^7\mathrm{Be}$ [1]. The reaction cross-section values are certainly important for nuclear data evaluation, for estimating the neutron spectrum in radiation testing of materials, and for considering the possibility of using lithium as the first wall of a fusion reactor. However, the data on cross-sections in the literature and databases differ significantly [2, 3]; for a number of reactions there are no data on the cross-section. Differences in the data from different authors are most likely due to the difficulty of determining the thickness of lithium layer due to its high chemical reactivity, which does not allow the use of some measurement methods. Our interest was in measuring the following reaction channels important for boron neutron capture therapy: ${}^6\mathrm{Li}(d,\alpha){}^4\mathrm{He}$, ${}^7\mathrm{Li}(d,\alpha){}^5\mathrm{He}$, and ${}^7\mathrm{Li}(d,n\alpha){}^4\mathrm{He}$ reactions.

The second group of reactions relates to the interaction of a proton with boron. The proton–boron fusion reaction is a potential candidate for the development of the so-called aneutronic fusion [4, 5], the process that can help avoiding the issues related to the high neutron flux generated in the most commonly employed deuterium–tritium reaction. The proton–boron fusion reaction is of interest both in nuclear astrophysics and in nuclear reaction analysis. More recently, this reaction has been proposed for the development of proton–boron capture therapy [6] and for the realization of α-particles sources using high energy and high intensity lasers [7]. This reaction is written as ${}^{11}\mathrm{B}(p,\alpha)\alpha\alpha$, ${}^{11}\mathrm{B}(p,3\alpha)$, or ${}^{11}\mathrm{B}(p,\alpha_0){}^8\mathrm{Be}$ and ${}^{11}\mathrm{B}(p,\alpha_1){}^8\mathrm{Be}^*$. The proton–boron fusion reaction has been studied since the 1930s [8, 9], but data from different authors differ. Obtaining the reliable experimental data on fundamental parameters (for example, direct or sequential decay, the cross-section, the energy spectrum of α-particles, the orbital angular momentum of α-particles) is still relevant. In this group of reactions we measured the following channels: ${}^{11}\mathrm{B}(p,\alpha_0){}^8\mathrm{Be}$ and ${}^{11}\mathrm{B}(p,\alpha_1){}^8\mathrm{Be}$.

The third group of reactions is about interaction of the deuteron with boron. This leads to numerous reactions, some of which have been studied in detail [10, 11], while others require some clarification. There are relatively few data on differential cross sections for deuteron-driven reactions on ${}^{10}\mathrm{B}$ and ${}^{11}\mathrm{B}$ at low energies. Such a study is quite relevant because of the roles these reactions play in several areas of applied physics, such as tokamak fusion plasma devices, as well as basic nuclear reaction theory. In addition to these areas of applied physics, these reactions can be used to test theories of nuclear reactions at low energies. We measured the cross-sections of the

* E-mail: G.M.Ostreinov@inp.nsk.su

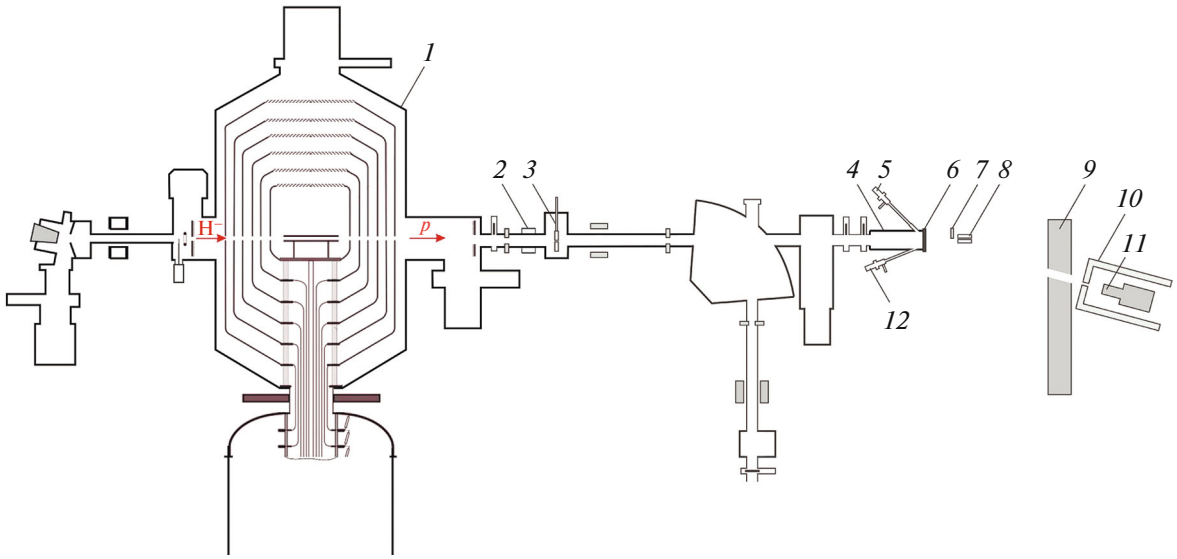

Fig. 1. Scheme of experimental facility: *1*—vacuum insulated tandem accelerator, *2*—contactless current sensor, *3*—cooled collimator, *4*—target unit, *5* and *12*—α spectrometer, *6*—lithium target, *7*—temporarily placed lead sheet, *8*—spectrometric radiometers of fast neutrons with diamond detector, *9*—temporarily mounted concrete wall, *10*—lead collimator, and *11*—γ spectrometer.

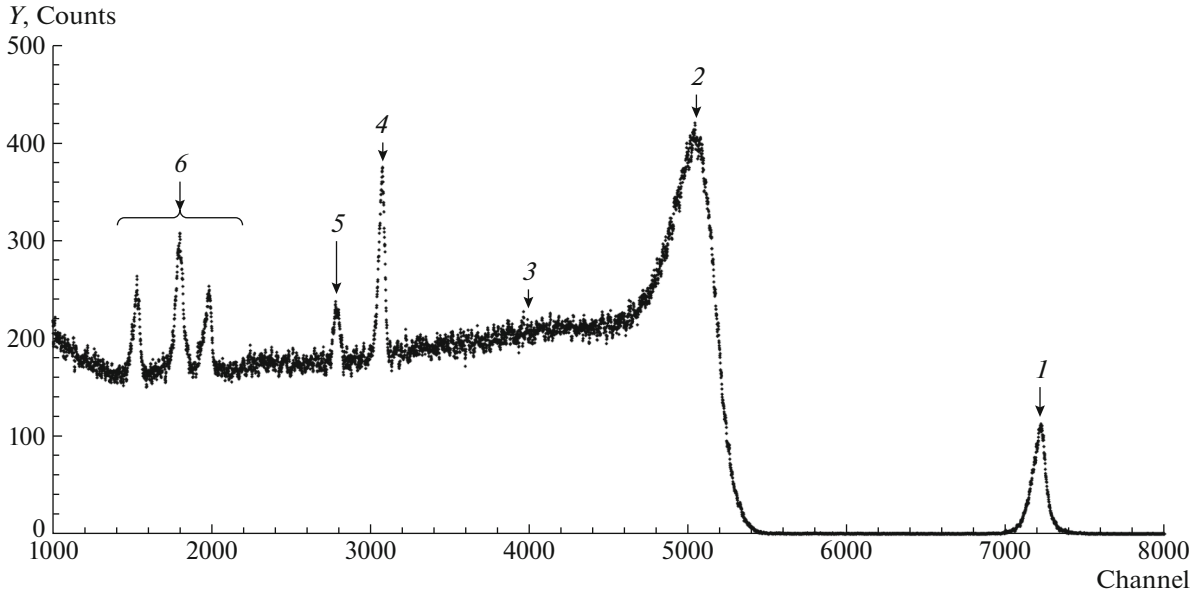

Fig. 2. The signal of the α-spectrometer at 0.6 MeV deuteron beam and 135° s, α—*1*—^{6}Li$(d,\alpha)^{4}$He reaction, *2*—^{7}Li$(d,\alpha)^{5}$He reaction α-particles, *3*—^{7}Li$(d,n\alpha)^{4}$He reaction α-particles, *4*—^{6}Li$(d,p_0)^{7}$Li reaction protons, *5*—^{6}Li$(d,p_1)^{7}$Li* reaction protons, *6*—^{12}C(d,p) reaction protons.

following nuclear reaction channels: ^{10}B$(d,\alpha_0)^{8}$Be, ^{10}B$(d,\alpha_1)^{8}$Be*, ^{11}B$(d,\alpha_0)^{9}$Be.

2. EXPERIMENTAL SETUP

The study was carried out at the accelerator-based neutron source VITA at Budker Institute of Nuclear Physics in Novosibirsk, Russia [12]. The layout of the experimental facility is shown in Fig. 1. The DC vacuum insulated tandem accelerator *1* is used to provide a deuteron and proton beam to direct it to target *4* through a 1 mm collimator *3*. The beam has the diameter of 5 mm on the surface of the target. The beam energy can vary within the range of 0.3–2.2 MeV, keeping the high-energy stability of 0.1%. The beam current can also vary in a wide range (from 0.5 to 10 mA) with the high current stability (0.4%). The beam current is measured and controlled

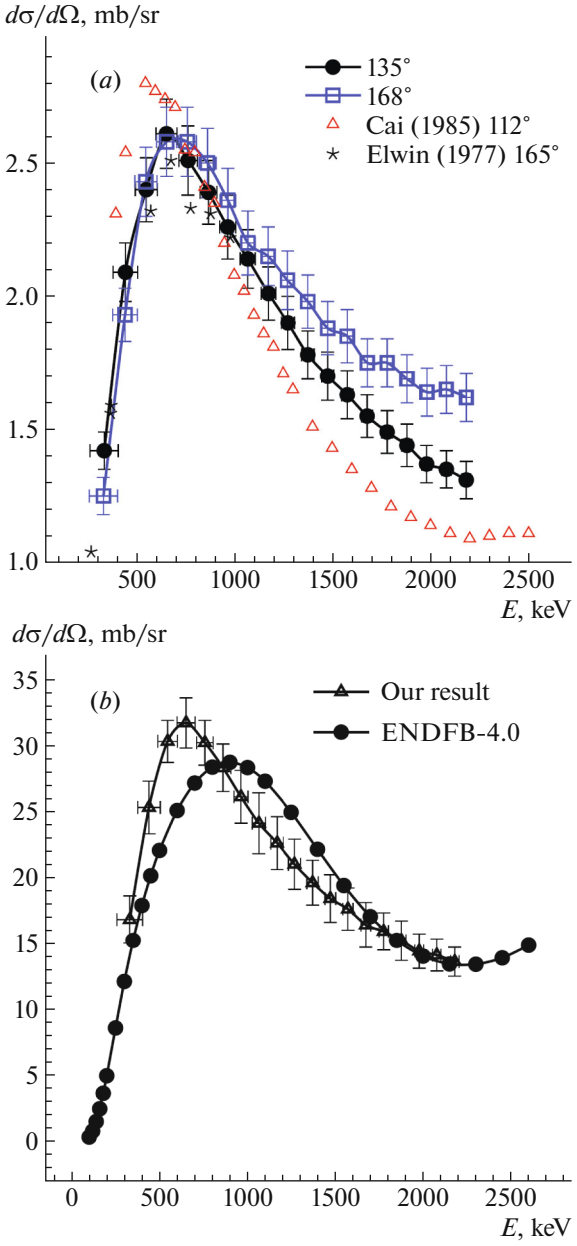

Fig. 3. (*a*) Differential cross section of ^{6}Li$(d,\alpha)\alpha$ reaction. (*b*) Full cross-section of ^{6}Li$(d,\alpha)\alpha$ reaction.

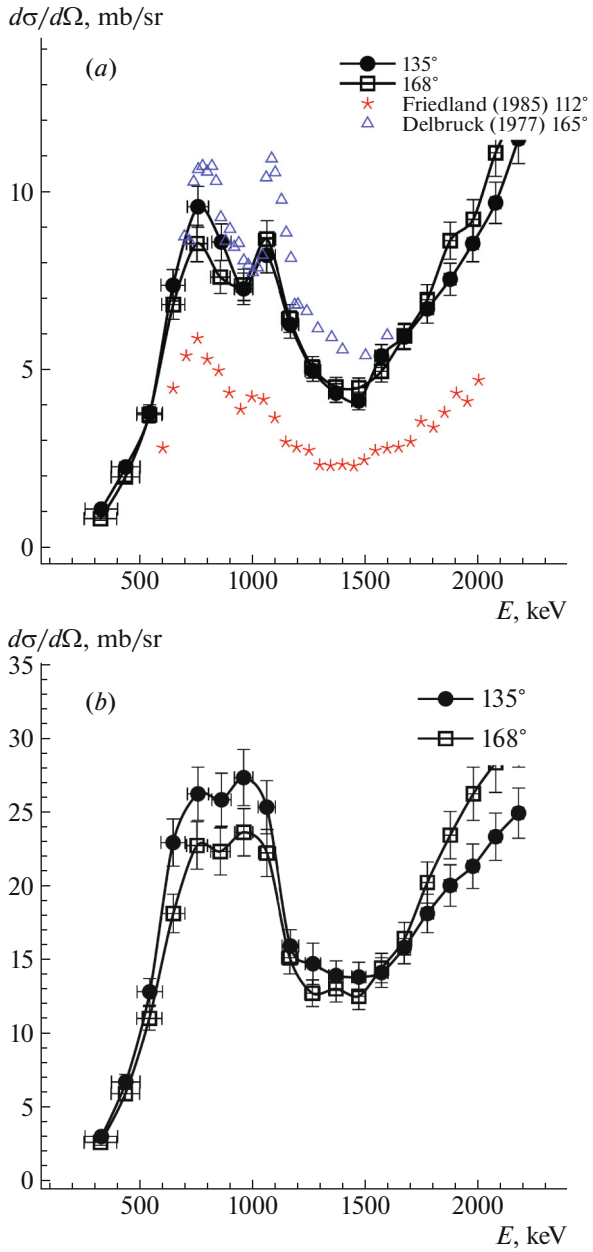

Fig. 4. (*a*) Differential cross-section of ^{7}Li$(d,\alpha)^{5}$He. (*b*) Differential cross-section of ^{7}Li$(d,n\alpha)\alpha$.

by a nondestructive DC current transformer NPCT (Bergoz Instrumentation, France) *2* and by a calibrated resistance connected to the target assembly, which is electrically isolated from the facility. Although the target assembly is made in the form of a deep Faraday cup, there is electron emission from it at a level of 1% of the ion current. Such electron emission increases the ion current by 1%, and this fact is taken into account. Vacuum evaporation of lithium or boron on the target was carried out at a separate stand. After deposition, closed with a gate valve to maintain vacuum inside the target assembly *4* was disconnected from the evaporation stand, transferred to the experimental facility, and connected to the horizontal beam line. We evaporated natural lithium, the used batch contained 99.956% of lithium. The percentage of lithium-7 in natural lithium varies from 92.41% to 92.58%; we will assume the lithium-7 content is equal to the average value, namely 92.5%. In cases of boron target the measured layer thickness is 1 μm with the heterogeneity of 5%. Taking into account all measurements and uncertainties, we will assume the boron layer thickness equal to $(9.0 \pm 0.9) \times 10^{18}$ atoms/cm^2 (0.7 ± 0.07 μm boron

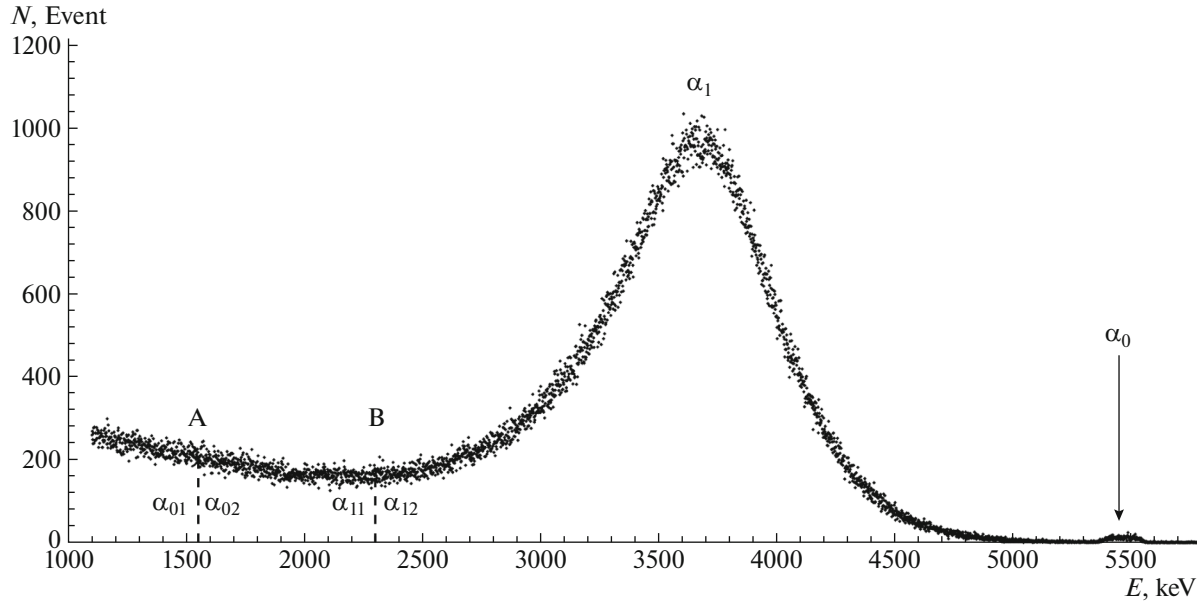

Fig. 5. The signal of the α-spectrometer at 1.5 MeV proton beam and 168°.

crystalline density). The content of ^{11}B isotope is considered equal to 80.2%.

3. DETECTOR AND CROSS SECTION MEASUREMENT

The intensity and energy of charged particles (reaction products) were measured by an α-spectrometer (*5* and *10* in Fig. 1) with silicon semiconductor detector PDPA-1 K (Institute of Physical and Technical Problems, Dubna, Russia). Sensitive surface area of the detector was $S = 20$ mm^2, energy resolution 13 keV, energy equivalent of noise 7 keV, capacity 30 pF, entrance window thickness 0.08 μm, standard natural background in the range of 3–8 MeV 0.15 imp/(cm^2 h). The α-spectrometer was calibrated with two standard radiation sources based on the plutonium-239 radionuclide. To determine the detection efficiency k of the α-spectrometer, the reference radiation sources were placed at the distance of 102.8 mm from the detector surface, and the activities were measured. We considered the detection efficiency of α-particles by the detector to be 100%, i.e. $k = 1$ with an accuracy of 3%. The energy calibration of the spectrometer was carried out with an exemplary spectrometric α-source with the ^{226}Ra isotope. It was established that the dependence of the energy E on a channel number N was linear and was described by the expression $E\,[\text{keV}] = 1.3941N + 82.003$. The measurements were carried out with two options for placing the α-spectrometer; in Fig. 1 they are shown as *5* and *12*. At the position *5* the α-spectrometer is placed at the angle of 135° at the distance of 722 mm from the place of generation of charged particles from lithium; at the position *12* the α-spectrometer is placed at the angle of 168° at the distance of 712 mm.

The cross-sections of the reactions were measured as follows. A thin layer of target was irradiated with a beam, and the α-spectrometer measured particles emitted at a certain solid angle. The differential cross-section of the reaction in the laboratory coordinates $d\sigma/d\Omega$ was found from the formula:

$$d\sigma/d\Omega = eY/(N \cdot k \cdot nl \cdot \Phi \cdot \Omega_{\text{lab}}), \qquad (1)$$

where e—is the elementary charge, Y—the experimental yield of α-particles (integrated peak counts), N—the number of measured charged particles in the reaction ($N = 3$), k—the efficiency of registration of α-particles by the spectrometer ($k = 1$), nl—the linear density target material nuclei, Φ— the beam fluence (accuracy of 1%), Ω_{lab} the solid angle ($\Omega_{\text{lab}} = 3.89 \times 10^{-5}$ at the angle of 135°; $\Omega_{\text{lab}} = 4.00 \times 10^{-5}$ at the angle of 168° with the accuracy of 5%). The relationship of the differential cross-section in the center-of-mass system $d\sigma_{\text{c.m.}}/d\Omega_{\text{c.m.}}$ and in the laboratory coordinates $d\sigma/d\Omega$ is given by the formula:

$$d\sigma_{\text{c.m.}}/d\Omega_{\text{c.m.}}$$
$$= |1 + \beta\cos\theta|/(1 + \beta^2 + 2\beta\cos\theta)^{3/2} d\sigma/d\Omega, \quad (2)$$

where $\beta = (m_p \cdot \tilde{M}/(M \cdot M_B) \cdot T_m/(T_m + Q))^{1/2}$, $T_m = E_p \cdot M/(m_p + M)$, M, $\tilde{M}$—the masses of the decay particles, m_p—the projectile mass, M_B—mass of the target particle, θ—the particle detection angle in the laboratory coordinates, in this case 135° or 168°, Q—released energy of reaction, E_p—the kinetic energy of incident projectile.

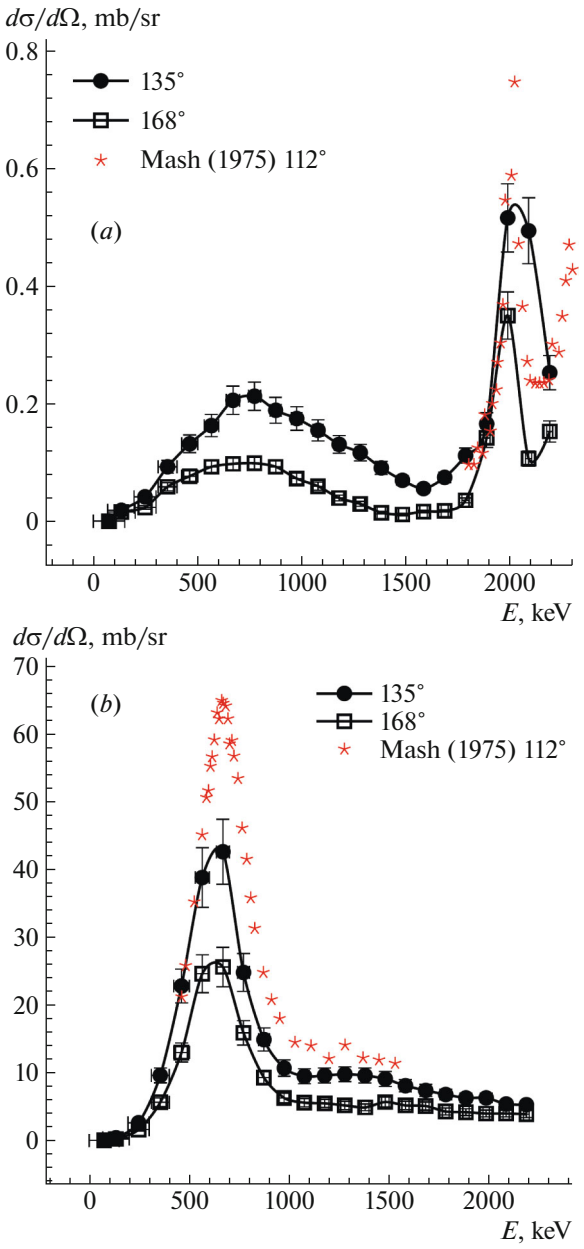

Fig. 6. (*a*) The measured differential cross-section of the $^{11}\mathrm{B}(p,\alpha_0)^8\mathrm{Be}$ reaction at 135° and 168°. Differential cross-sections are in the center-of-mass system. (*b*) The measured differential cross-section of the $^{11}\mathrm{B}(p,\alpha_1)^8\mathrm{Be}^*$ reaction at 135° and 168°. Differential cross-sections are in the center-of-mass system.

4. d + Li REACTIONS

A typical spectrum is shown in Figs. 2. The narrow high-energy peak corresponds to alpha particles from the reaction $^6\mathrm{Li}(d,\alpha)^4\mathrm{He}$. Narrow single peaks in the low-energy region correspond to (d,p) reactions with various target components. According to the energy and excitation function, these peaks were found to be related to reactions with emission protons: $^{16}\mathrm{O}(d,p_1)$, $^{16}\mathrm{O}(d,p_0)$, $^{12}\mathrm{C}(d,p_0)$, where indices 0, 1 correspond to the ground and first excited states of the recoil nucleus. In addition to the narrow peaks, the entire spectrum range contains a broad uniform distribution with a single broad peak at its upper end. The $^6\mathrm{Li}(d,\alpha)^4\mathrm{He}$ reaction produces two α-particles with the same high energy, and, therefore, α-particles are easily identified in the measured energy spectrum of charged particles (see *1* in Fig. 2). The data obtained make it possible to determine the differential cross-section of the $^6\mathrm{Li}(d,\alpha)^4\mathrm{He}$ reaction; it is given in Fig. 3*a*. At high deuteron energies, double events from other reactions and products of the $^6\mathrm{Li}(d,\alpha)^4\mathrm{He}$ reaction from deuterons with half the energy appear in the region of this peak. However, these contributions are small and easy to estimate. The cross section of the $^6\mathrm{Li}(d,\alpha)^4\mathrm{He}$ reaction σ is presented in Fig. 3*a* in comparison with ENDF/B-VIII.0. The $^7\mathrm{Li}(d,\alpha)^5\mathrm{He}$ reaction produces α-particles detected by the α-spectrometer (see *2* in Fig. 2). This peak is clearly identified. The resulting ^{5}He atomic nucleus almost instantly decays into a neutron and an α-particle. The energy spectrum of these α-particles is wider: from 3 to 7 MeV. The differential cross-section of the $^7\mathrm{Li}(d,\alpha)^5\mathrm{He}$ reaction is given in Fig. 4*a*. The differential cross section of the reaction $\mathrm{Li}(d,n\alpha)^4\mathrm{He}$ is given in Fig. 4*b*.

5. $p + {}^{11}$B REACTIONS

A typical spectrum from the α-spectrometer is shown in Fig. 5. The signal in channels below 1 MeV is due to the protons backscattered from the copper substrate of the boron target, including double events. The sharp peak in the energy region of 5.5 MeV corresponds to primary α-particles of the $^{11}\mathrm{B}(p,\alpha_0)^8\mathrm{Be}$ reaction (designated as α_0). Secondary particles of this reaction, α_{01} and α_{02}, are grouped in the energy region of 1.4 MeV. On the graph, dashed line is drawn to separate these secondary particles. We can say that if one secondary particle has the energy above 1.4 MeV, then the other has a lower energy. Relative to this line, α-particles are distributed in the energy range of the order of $\pm$0.5 MeV. The wide peak in the energy region of 3.7 MeV corresponds to the primary α-particles of the $^{11}\mathrm{B}(p,\alpha_1)^8\mathrm{Be}^*$ reaction (designated as α_1). Secondary particles of this reaction, α_{11} and α_{12}, are grouped in the energy region of 2.4 MeV (line B). We can also say that if one secondary particle has the energy above 2.4 MeV, then the other has a lower energy. This statement is important for us to calculate the total number of α-particles in the $^{11}\mathrm{B}(p,\alpha_1)^8\mathrm{Be}^*$ reaction. In this reaction, two of the three α-particles have energies above 2.4 MeV (line B), one below. Counting the number of α-particles with energies below 2.4 MeV is

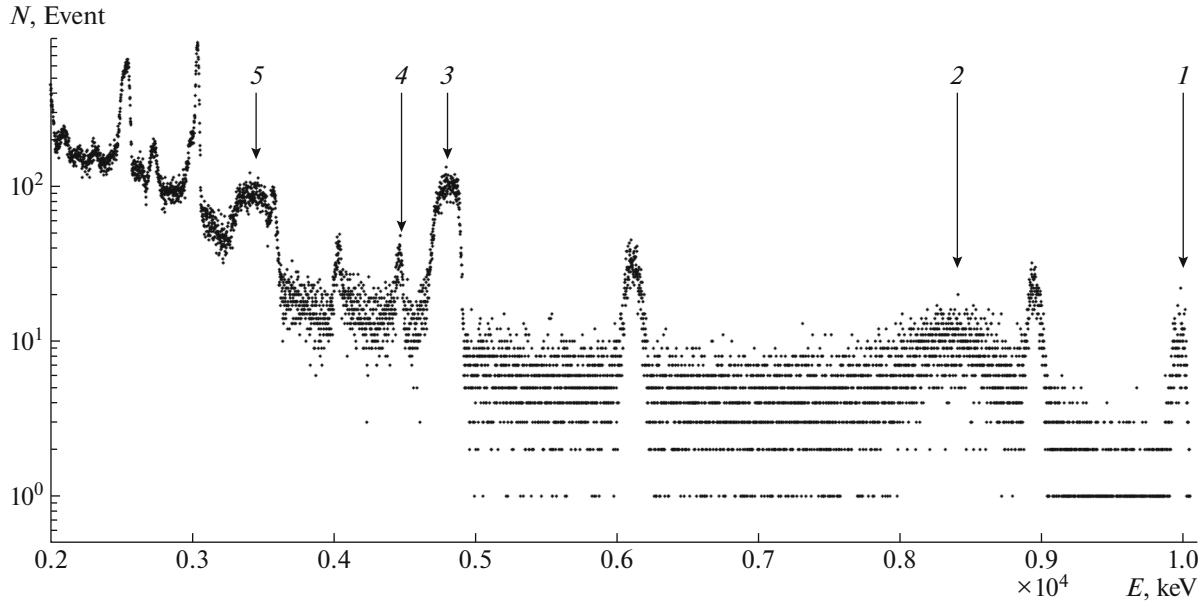

Fig. 7. The signal of the α-spectrometer at 1.5 MeV deuteron beam and 135°: *1*—^{10}B$(d,\alpha_0)^8$Be reaction α-particles, *2*—^{10}B$(d,\alpha_1)^8$Be* reaction α-particles, *3*—^{11}B$(d,\alpha_0)^9$Be reaction α-particles, *4*—^{10}B$(d,p_2)^{11}$B* reaction protons, *5*—^{11}B$(d,\alpha_2)^9$Be* reaction α-particles.

difficult due to the presence of backscattered protons, secondary α-particles of the ^{11}B$(p,\alpha_0)^8$Be reaction, and α-particles of the ^{10}B$(p,\alpha)^7$Be reaction. Therefore, we will count the number of α-particles with the energy above 2.4 MeV (this energy varies slightly with the proton energy and the angle of detection) and multiply by 3/2 in order to determine the total number of α-particles in the ^{11}B$(p,\alpha_1)^8$Be* reaction. The differential cross-sections of the ^{11}B$(p,\alpha_0)^8$Be and ^{11}B$(p,\alpha_1)^8$Be* reaction; are given in Fig. 6*a* and Fig. 6*b*. The accuracy of the cross-section measurement is determined by the accuracy of the boron thickness determination (10%), the accuracy of the proton fluence determination (1%), the accuracy of the solid angle determination (5%), and the statistical uncertainty (2–30%); in total it is 12–33%.

6. d + B REACTIONS

The reaction of interaction of a deuteron with boron-10 nucleus forming protons can occur either as a sequential decay via the ground state of ^{11}B, ^{10}B$(d,p_0)^{11}$B, or via six excited states, ^{10}B$(d,p_{1-6})^{11}$B*. A typical spectrum from the α-spectrometer is shown in Fig. 7. The accuracy of cross section measurement is determined by the accuracy of boron thickness determination (10%), the accuracy of deuteron fluence determination (1%), the accuracy of solid angle determination (5%), and statistical uncertainty (9–34%); in total it is 11–34%. Differential cross-section of the ^{10}B$(d,\alpha_0)^8$Be reaction is given in Fig. 8*a*. It is noticeable that the reaction proceeds non isotropically. The differential cross-section of the ^{11}B$(p,\alpha_0)^9$Be reaction is given in Fig. 8*b*. The accuracy of cross-section measurement is determined by the accuracy of boron thickness determination (10%), the accuracy of deuteron fluence determination (1%), the accuracy of solid angle determination (5%), the accuracy in counting the number of events at energies above 1.4 MeV (3%), and statistical uncertainty (2–32%); in total it is 12–32%. The differential cross-section of the ^{10}B$(d,\alpha_1)^8$Be* reaction is given in Fig. 9. In comparison of data from [13] where this reaction was measured at the angle 156°, a small resonance peak in the region of 1.7 MeV in our data is not clearly visible and cross-section values are several times lower. The authors in [13] indicate an error in the cross-section measurement of 14%, but a direct comparison with our data is not correct due to the anisotropy of the reaction in the center-of-mass system. On the other hand, the measurements in article [14] agree well with our data within the error limits. The accuracy of cross-section measurement is determined by the accuracy of boron thickness determination (10%), the accuracy of deuteron fluence determination (1%), the accuracy of solid angle determination (5%), the accuracy in counting the number of events at energies above 1.4 MeV (3%), and statistical uncertainty (5–

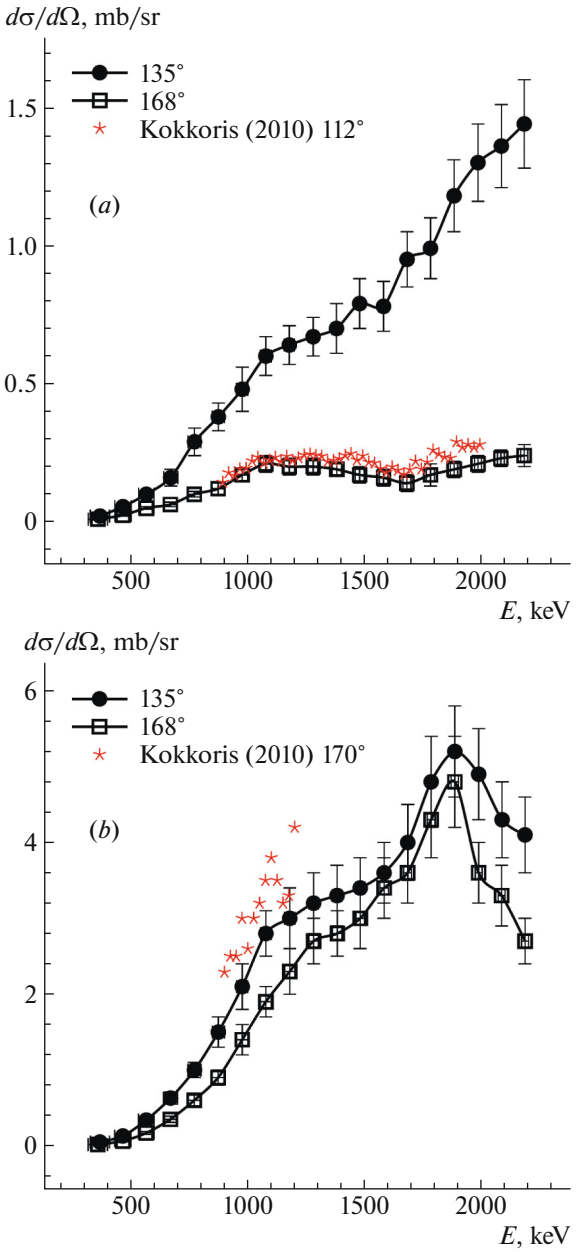

Fig. 8. (*a*) The measured differential cross-section of the ^{10}B$(d, \alpha_0)^8$Be reaction. Differential cross-sections are in the center-of-mass system. (*b*) The measured differential cross-section of the ^{11}B$(d, \alpha_0)^9$Be.

15%); in total it is 15%. We assume, based on the obtained data, that this cross section is characterized by non-isotropy.

7. CONCLUSION

Differential cross sections of three groups of reactions in the energy range of 0.2–2.5 MeV, initiated by proton and deuteron beams, were measured for two angles of 135° and 168° with high accuracy . For the $d + $Li reaction, comparison with existing databases showed good agreement of the results. The reaction channel Li$(d, n\alpha)^4$He was measured for the first time. For $p + ^{11}$B was measured the energy spectrum of the reaction products. The shape of the energy spectrum of the reaction products indicates that the reaction with the formation of three α-particles proceeds predominantly via the ground state of ^{8}Be, ^{11}B$(p, \alpha_0)^8$Be, or via the first excited state, ^{11}B$(p, \alpha_1)^8$Be*. The direct decay probability is 2000–3000 times less than the sequential decay probability. The obtained data allowed us to determine the differential cross-sections of the reactions, the angular distribution of the α-particles' emission, and the total reaction cross-section with high accuracy and reliability. The deuteron–boron fusion

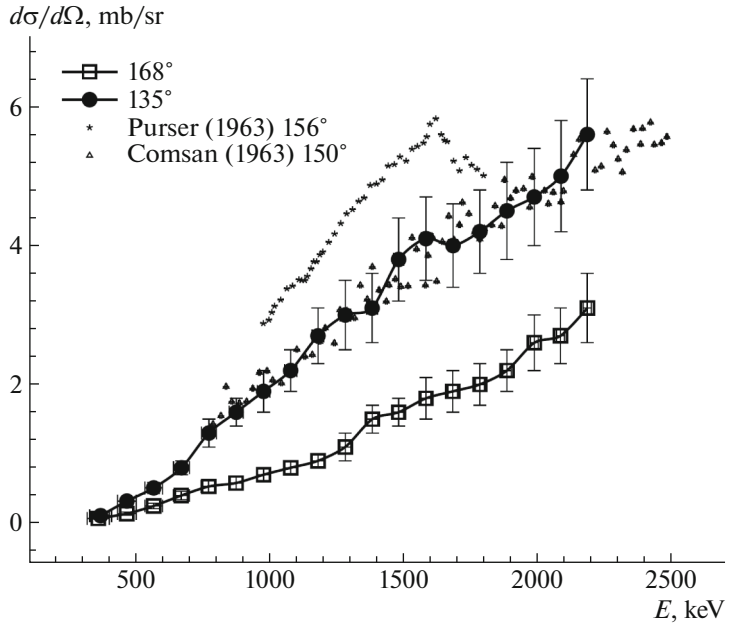

Fig. 9. Differential cross section of $^{10}B(d, \alpha_1)^8Be^*$ reaction.

reaction produces many different charged particles. Data on the reactions' cross-sections differ among different authors. We measured the energy spectrum of the reaction products of the deuteron–boron interaction at deuteron energies up to 2.2 MeV for two angles of 135° and 168°. The obtained data allowed us to determine the differential cross-sections of the $^{10}B(d, \alpha_0)^8Be$, $^{10}B(d, \alpha_1)^8Be^*$, $^{11}B(d, \alpha_0)^9Be$, reactions.

FUNDING

The study was supported by the Russian Science Foundation, grant no. 19-72-30005, https://rscf.ru/project/19-72-30005/.

CONFLICT OF INTEREST

The authors of this work declare that they have no conflicts of interest.

REFERENCES

1. S. Y. Taskaev, Phys. Part. Nucl. **46**, 956 (2015). https://doi.org/10.1134/s1063779615060064
2. A. J. Elwyn, R. E. Holland, C. N. Davids, L. Meyer-Schutzmeister, J. E. Monahan, F. P. Mooring, and W. Ray, Phys Rev. C **16**, 1744 (1977). https://doi.org/10.1103/physrevc.16.1744
3. W. Whaling and T. W. Bonner, Phys. Rev. **79**, 258 (1950). https://doi.org/10.1103/physrev.79.258
4. N. Rostoker, M. W. Binderbauer, and H. J. Monkhorst, Science **278**, 1419 (1997). https://doi.org/10.1126/science.278.5342.1419
5. Johnm. M. Dawson, in *Fusion: Magnetic Confinement, Part B*, Ed. by E. Teller (Academic, 1981), p. 453. https://doi.org/10.1016/b978-0-12-685241-7.50013-x
6. G. A. P. Cirrone, L. Manti, D. Margarone, G. Petringa, L. Giuffrida, A. Minopoli, A. Picciotto, G. Russo, F. Cammarata, P. Pisciotta, F. M. Perozziello, F. Romano, V. Marchese, G. Milluzzo, V. Scuderi, G. Cuttone, and G. Korn, Sci. Rep. **8**, 1141 (2018). https://doi.org/10.1038/s41598-018-19258-5
7. J. Bonvalet, P. H. Nicolaï, D. Raffestin, E. D'humieres, D. Batani, V. Tikhonchuk, V. Kantarelou, L. Giuffrida, M. Tosca, G. Korn, A. Picciotto, A. Morace, Y. Abe, Y. Arikawa, S. Fujioka, Y. Fukuda, Y. Kuramitsu, H. Habara, and D. Margarone, Phys. Rev. E **103**, 53202 (2021). https://doi.org/10.1103/physreve.103.053202
8. M. L. E. Oliphant and E. Rutherford, Proc. R. Soc. London A **141**, 259 (1933). https://doi.org/10.1098/rspa.1933.0117
9. Ph. I. Dee and C. W. Gilbert, Proc. R. Soc. London A **154**, 279 (1936). https://doi.org/10.1098/rspa.1936.0051
10. J. Yan, F. E. Cecil, J. A. Mcneil, M. A. Hofstee, and P. D. Kunz, Phys Rev. C **55**, 1890 (1997). https://doi.org/10.1103/physrevc.55.1890

11. F. E. Cecil and R. F. Fahlsing, Phys Rev. C **24**, 1769 (1981). https://doi.org/10.1103/physrevc.24.1769
12. S. Taskaev, E. Berendeev, M. Bikchurina, T. Bykov, D. Kasatov, I. Kolesnikov, A. Koshkarev, A. Makarov, G. Ostreinov, V. Porosev, S. Savinov, I. Shchudlo, E. Sokolova, I. Sorokin, T. Sycheva, and G. Verkhovod, Biology **10**, 350 (2021). https://doi.org/10.3390/biology10050350
13. K. H. Purser and B. H. Wildenthal, Nuclear Physics **44**, 22 (1963). https://doi.org/10.1016/0029-5582(63)90003-8
14. M. N. H. Comsan, M. A. Farouk, A. A. Elkamhaw, M. S. Eltahawy, and A. N. Lvov, Atomkernenergie **13**, 415 (1968).